

Highly Efficient and Stable Inverted Polymer Solar Cells Integrated with a Cross-Linked Fullerene Material as an Interlayer

Chao-Hsiang Hsieh, Yen-Ju Cheng,* Pei-Jung Li, Chiu-Hsiang Chen, Martin Dubosc, Ru-Meng Liang, and Chain-Shu Hsu*

Department of Applied Chemistry, National Chiao Tung University, 1001 Ta Hsueh Road Hsin-Chu, 30010 Taiwan

Received January 11, 2010; E-mail: yjcheng@mail.nctu.edu.tw; cshsu@mail.nctu.edu.tw

Abstract: A novel PCBM-based n-type material, [6,6]-phenyl-C₆₁-butyric styryl dendron ester (PCBSD), functionalized with a dendron containing two styryl groups as thermal cross-linkers, has been rationally designed and easily synthesized. In situ cross-linking of PCBSD was carried out by heating at a low temperature of 160 °C for 30 min to generate a robust, adhesive, and solvent-resistant thin film. This cross-linked network enables a sequential active layer to be successfully deposited on top of this interlayer to overcome the problem of interfacial erosion and realize a multilayer inverted device by all-solution processing. An inverted solar cell device based on an ITO/ZnO/C-PCBSD/P3HT:PCBM/PEDOT:PSS/Ag configuration not only achieves enhanced device characteristics, with an impressive PCE of 4.4%, but also exhibits an exceptional device lifetime without encapsulation; it greatly outperforms a reference device (PCE = 3.5%) based on an ITO/ZnO/P3HT:PCBM/PEDOT:PSS/Ag configuration without the interlayer. This C-PCBSD interlayer exerts multiple positive effects on both P3HT/C-PCBSD and PCBM/C-PCBSD localized heterojunctions at the interface of the active layer, including improved exciton dissociation efficiency, reduced charge recombination, decreased interface contact resistance, and induction of vertical phase separation to reduce the bulk resistance of the active layer as well as passivation of the local shunts at the ZnO interface. Moreover, this promising approach can be applied to another inverted solar cell, ITO/ZnO/C-PCBSD/PCPDTBT:PC₇₁BM/PEDOT:PSS/Ag, using PCPDTBT as the p-type low-band-gap conjugated polymer to achieve an improved PCE of 3.4%. Incorporation of this cross-linked C₆₀ interlayer could become a standard procedure in the fabrication of highly efficient and stable multilayer inverted solar cells.

Introduction

Polymeric solar cells (PSCs) have emerged as a promising alternative technique for producing clean and renewable energy due to their potential for fabrication onto large areas of lightweight flexible substrates by low-cost solution processing. To maximize the donor–acceptor heterojunction interfacial area for efficient exciton dissociation, mainstream PSC devices adopt the concept of a bulk heterojunction (BHJ), where an active layer contains a p-type donor and an n-type acceptor to form an interpenetrating nanoscale network.¹ A conventional BHJ PSC with an active layer sandwiched by a low-work-function aluminum cathode and a hole-conducting poly(3,4-ethylenedioxythiophene):poly(styrenesulfonic acid) (PEDOT:PSS) layer on top of an indium tin oxide substrate is the most widely used and investigated device configuration. On the basis of this device architecture, high power-conversion efficiencies (PCEs)

of ca. 4–5% have been achieved using a blend consisting of a regioregular poly(3-hexylthiophene) (P3HT) and a fullerene derivative, [6,6]-phenyl-C₆₁-butyric acid methyl ester (PCBM).² Along with high performance, long-term stability is a growing concern for PSCs. However, it is highly challenging to develop a PSC that can achieve a high PCE while maintaining good ambient stability of the device. Prolonged exposure to air rapidly reduces the performance of unencapsulated conventional devices. Many mechanisms are proposed to explain the decay. First, oxygen and moisture can diffuse to the active layer through grain boundaries and pinholes in the metal electrode, which in turn degrades the organic active materials. Second, due to direct contact, the aluminum electrode can easily penetrate the active layer, leading to chemical reactions and alteration of the intrinsic properties of semiconductors. As a result, metal oxides such as a titanium oxide or zinc oxide buffer layer have been inserted between the organic active layer and the Al electrode to improve

(1) (a) Yu, G.; Gao, J.; Hummelen, J. C.; Wudl, F.; Heeger, A. J. *Science* **1995**, *270*, 1789. (b) Halls, J. J. M.; Walsh, C. A.; Greenham, N. C.; Marseglia, E. A.; Friend, R. H.; Moratti, S. C.; Holmes, A. B. *Nature* **1995**, *376*, 498. (c) Thompson, B. C.; Fréchet, J. M. J. *Angew. Chem., Int. Ed.* **2008**, *47*, 58. (d) Günes, S.; Neugebauer, H.; Sariciftci, N. S. *Chem. Rev.* **2007**, *107*, 1324. (e) Brabec, C. J.; Sariciftci, N. S.; Hummelen, J. C. *Adv. Funct. Mater.* **2001**, *11*, 15. (f) Coakley, K. M.; McGehee, M. D. *Chem. Mater.* **2004**, *16*, 4533. (g) Cheng, Y.-J.; Yang, S.-H.; Hsu, C.-S. *Chem. Rev.* **2009**, *109*, 5868.

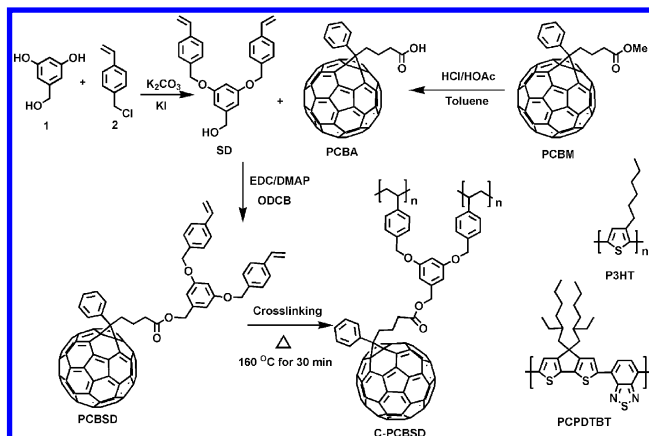
(2) (a) Woo, C. H.; Thompson, B. C.; Kim, B. J.; Toney, M. F.; Fréchet, J. M. J. *J. Am. Chem. Soc.* **2008**, *130*, 16324. (b) Reyes-Reyes, M.; Kim, K.; Carroll, D. L. *Appl. Phys. Lett.* **2005**, *87*, 083506. (c) Li, G.; Yao, Y.; Yang, H.; Shrotriya, V.; Yang, G.; Yang, Y. *Adv. Funct. Mater.* **2007**, *17*, 1636. (d) Li, G.; Shrotriya, V.; Huang, J.; Yao, Y.; Moriarty, T.; Emery, K.; Yang, Y. *Nat. Mater.* **2005**, *4*, 864. (e) Mayer, A. C.; Scully, S. R.; Hardin, B. E.; Rowell, M. W.; McGehee, M. D. *Mater. Today* **2007**, *10*, 28. (f) Ma, W.; Yang, C.; Gong, X.; Lee, K.; Heeger, A. J. *Adv. Funct. Mater.* **2005**, *15*, 1617.

device stability by providing hole blocking and an oxygen barrier.³ Nevertheless, the most serious problem responsible for device instability is rapid oxidation of the Al electrode.⁴ A more effective approach to circumvent this problem is to fabricate so-called inverted devices.⁵ By taking advantage of the ability to reverse the polarity of charge collection in an inverted configuration, air-stable high-work-function metal Ag can substitute for air-sensitive Al as the anodic electrode for hole collection, while metal oxides TiO₂ and ZnO act as the electron-selective contact at the ITO interface. Despite dramatic improvement in the operational lifetime, inverted solar cells still suffer from a trade-off between stability and performance. Recently reported inverted devices based on P3HT/PCBM composite exhibited PCEs in the range of ca. 2–4%, which is inferior to that of regular solar cells, presumably due to poor electrical coherence at the organic/inorganic interfaces.^{5f–h,6}

Self-organization of a fluorinated PCBM buffer layer on top of a P3HT/PCBM active layer has been shown to improve the photovoltaic performance of a regular PSC.⁷ It is believed that incorporating an additional n-type C₆₀ derivative interlayer between the inorganic metal oxide and the organic active layer in an inverted solar cell might improve device performance by modulating the electronic and orbital interactions at the upper and bottom interfaces.

The major obstacle to realizing such a multilayer inverted device by cost-effective solution processing is that the deposited C₆₀ derivative interlayer must possess sufficient resistance against the organic solvent used in processing the sequential active layer to prevent interfacial erosion.⁸ A C₆₀ derivative having a carboxylic acid group that forms a self-assembled monolayer (SAM) on the metal oxide surface has been successfully used to enhance the device characteristics.^{5c,9} The potential drawbacks for SAM formation are incomplete coverage at the molecular scale and probable desorption of this monolayer during wet processing, creating localized defects in this interlayer.¹⁰ Very recently, a cross-linkable polythiophene has been successfully used to improve the thermal stability of a PCS by

Scheme 1. Synthetic Route of PCBSD and Chemical Structures of C-PCBSD, P3HT, and PCPDTBT



chemically fixing the optimized morphology of the active layer.¹¹ Moreover, this cross-linking approach also allows for fabricating a bilayer solar cell device by solution processing.¹¹ As a result, development of a fullerene material that can be solution-deposited on a substrate and readily undergo chemical cross-linking to form a robust and immobilized layer could be a straightforward and ideal strategy. With this distinct interlayer, mutual diffusion between the upper active layer and the bottom metal oxide layer, leading to direct contact, can be avoided. Styrene is known to be a superb thermally curable group because it can undergo rapid polymerization in the solid state to form polystyrene without the use of any initiators.¹² Therefore, we have designed and synthesized a fullerene derivative, [6,6]-phenyl-C₆₁-butyric styryl dendron ester (PCBSD), that contains a small dendron functionalized with two thermally cross-linkable styryl groups. Herein, we report a generally applicable and effective approach that integrates an interlayer of this cross-linked PCBSD (C-PCBSD) into inverted solar cells, achieving not only superior device performance but also remarkable long-term stability.

Results and Discussion

In the presence of 1-ethyl-3-(3-(dimethylamino)propyl)carbodiimide (EDC) and 4-(dimethylamino)pyridine (DMAP), PCBSD was easily prepared by esterification of styrene-containing dendron SD with [6,6]-phenyl-C₆₁-butyric acid (PCBA), which was obtained by the hydrolysis of PCBM (Scheme 1).¹³ The core structure of PCBSD is based on the most widely used n-type material, PCBM; therefore, PCBSD is expected to inherit all the excellent electrical properties of its parent, PCBM.

The thermal transition properties of PCBSD monomer were investigated by the first scan of differential scanning calorimetry (DSC). It showed a broad exothermic peak with a *T*_{max} value around 149 °C, which clearly indicates thermal cross-linking of styrene groups (Figure S1, Supporting Information). In

- (3) (a) Lee, K.; Kim, J. Y.; Park, S. H.; Kim, S. H.; Cho, S.; Heeger, A. J. *Adv. Mater.* **2007**, *19*, 2445. (b) Gilot, J.; Barbu, I.; Wienk, M. M.; Janssen, R. A. J. *Appl. Phys. Lett.* **2007**, *91*, 113520. (c) Yang, C.; Kim, J. Y.; Cho, S.; Lee, J. K.; Heeger, A. J.; Wudl, F. *J. Am. Chem. Soc.* **2008**, *130*, 6444. (d) Yip, H.-L.; Hau, S. K.; Baek, N. S.; Ma, H.; Jen, A. K.-Y. *Adv. Mater.* **2008**, *20*, 2376. (e) Kim, J. Y.; Kim, S. H.; Lee, H.-H.; Lee, K.; Ma, W.; Gong, X.; Heeger, A. J. *Adv. Mater.* **2006**, *18*, 572.
- (4) Sahin, Y.; Alem, S.; de Bettignies, R.; Nunzi, J.-M. *Thin Solid Films* **2005**, *476*, 340.
- (5) (a) Li, G.; Chu, C.-W.; Shrotriya, V.; Huang, J.; Yang, Y. *Appl. Phys. Lett.* **2006**, *88*, 253503. (b) Hau, S. K.; Yip, H.-L.; Baek, N. S.; Zou, J.; O'Malley, K.; Jen, A. K.-Y. *Appl. Phys. Lett.* **2008**, *92*, 253301. (c) Hau, S. K.; Yip, H.-L.; Acton, O.; Baek, N. S.; Ma, H.; Jen, A. K.-Y. *J. Mater. Chem.* **2008**, *18*, 5113. (d) Liao, H.-H.; Chen, L.-M.; Xu, Z.; Li, G.; Yang, Y. *Appl. Phys. Lett.* **2008**, *92*, 173303. (e) Waldauf, C.; Morana, M.; Denk, P.; Schilinsky, P.; Coakley, K.; Choulis, S. A.; Brabec, C. J. *Appl. Phys. Lett.* **2006**, *89*, 233517. (f) Mor, G. K.; Shankar, K.; Paulose, M.; Varghese, O. K.; Grimes, C. A. *Appl. Phys. Lett.* **2007**, *91*, 152111. (g) White, M. S.; Olson, D. C.; Shaheen, S. E.; Kopidakis, N.; Ginley, D. S. *Appl. Phys. Lett.* **2006**, *89*, 143517. (h) Yu, B.-Y.; Tsai, A.; Tsai, S.-P.; Wong, K.-T.; Yang, Y.; Chu, C.-W.; Shyue, J.-J. *Nanotechnology* **2008**, *19*, 255202.
- (6) Steim, R.; Choulis, S. A.; Schilinsky, P.; Brabec, C. J. *Appl. Phys. Lett.* **2008**, *92*, 093303.
- (7) Wei, Q.; Nishizawa, T.; Tajima, K.; Hashimoto, K. *Adv. Mater.* **2008**, *20*, 2211.
- (8) (a) Liang, C.-W.; Su, W.-F.; Wang, L. *Appl. Phys. Lett.* **2009**, *95*, 133303. (b) Huang, J.-S.; Chou, C.-Y.; Lin, C.-F. *Sol. Energy Mater. Sol. Cells* **2010**, *94*, 182.
- (9) Hau, S. K.; Yip, H.-L.; Ma, H.; Jen, A. K.-Y. *Appl. Phys. Lett.* **2008**, *93*, 233304.

- (10) Goh, C.; Scully, S. R.; McGehee, M. D. *J. Appl. Phys.* **2007**, *101*, 114503.
- (11) Kim, B. J.; Miyamoto, Y.; Ma, B.; Fréchet, J. M. J. *Adv. Funct. Mater.* **2009**, *19*, 2273.
- (12) (a) Cheng, Y.-J.; Liu, M. S.; Zhang, Y.; Niu, Y.; Huang, F.; Ka, J.-W.; Yip, H.-L.; Tian, Y.; Jen, A. K.-Y. *Chem. Mater.* **2008**, *20*, 413. (b) Huang, F.; Cheng, Y.-J.; Zhang, Y.; Liu, M. S.; Jen, A. K.-Y. *J. Mater. Chem.* **2008**, *18*, 4495.
- (13) Hummelen, J. C.; Knight, B. W.; LePeg, F.; Wudl, F. *J. Org. Chem.* **1995**, *60*, 532.

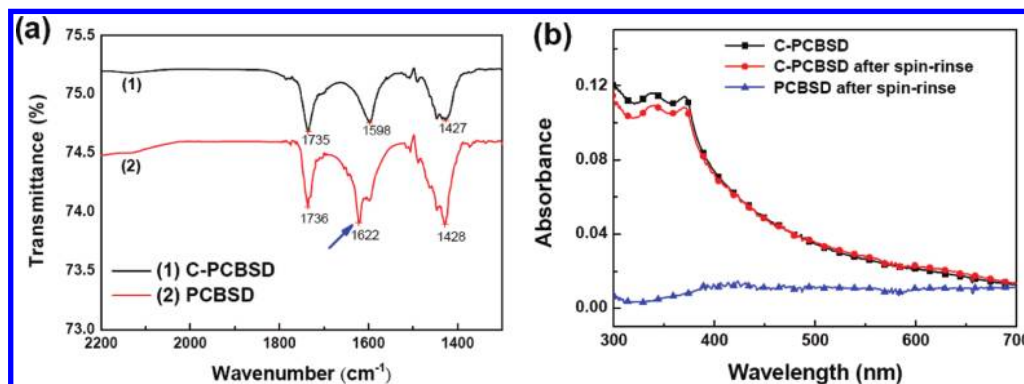


Figure 1. (a) Infrared spectra of the PCBSD precursor and cross-linked PCBSD thin film. (b) Absorption spectra of the cross-linked PCBSD before (squares) and after (circles) rinsing with dichlorobenzene and non-cross-linked PCBSD layer after rinsing with dichlorobenzene (triangles).

addition, the vibrational stretching of the vinyl groups at 1622 cm^{-1} in the PCBSD completely disappears in the IR spectrum after the thermal treatment, again undoubtedly proving the occurrence of cross-linking (Figure 1a). These results reveal that the two arms of the dendron provide adequate flexibility for styryl groups to react in the solid state. After the initial heating cycle, a high T_g value of ca. $142\text{ }^\circ\text{C}$ was observed during the second DSC heating, indicating that the resultant C-PCBSD is highly amorphous. Additionally, the cross-linked network prevents the diffusion of PCBSD molecules, which can reduce the tendency toward crystallization and maintain long-term morphological stability of the fullerene film (Figure S1).¹⁴ In spite of its cross-linkable property, PCBSD can be stably stored at room temperature without the need for nitrogen protection.

After the thermal cross-linking condition of PCBSD was determined, a multilayer inverted solar cell device A based on the configuration ITO/ZnO/C-PCBSD/P3HT:PCBM(1:1, w/w)/PEDOT:PSS/Ag was fabricated. The electron-selective layer of ZnO nanoparticles was first prepared on ITO according to the literature.¹⁵ A solution of PCBSD was spin-coated on top of the ZnO surface, followed by thermal curing at $160\text{ }^\circ\text{C}$ for 30 min.

To prove that the cross-linked network of PCBSD is unambiguously generated on top of the ZnO, atomic force microscopy (AFM) and contact angle measurements were performed (Figure 2a,b). The bare ZnO/ITO surface exhibited a root-mean-square (rms) roughness of 3.16 nm and a wetting angle to DI water of 42° . After a layer of cross-linked PCBSD was deposited on top of the ZnO/ITO, the surface roughness decreased significantly to 0.6 nm, and the contact angle increased to 95° (Figure S2). These results reveal that voids in the uneven ZnO nanostructure surface are completely filled and covered by the PCBSD to form a smoother and more hydrophobic surface. By using an α -step profilometer, the thickness of the cross-linked layer is estimated to be approximately 10 nm, which indicates that the thin film consists of multiple layers of PCBSD molecules. Most importantly, this cross-linked network produced a robust and adhesive thin film with sufficient solvent resistance, evidenced by the almost unchanged absorption spectra measured before and after rinsing with dichlorobenzene (Figure 1b). Note

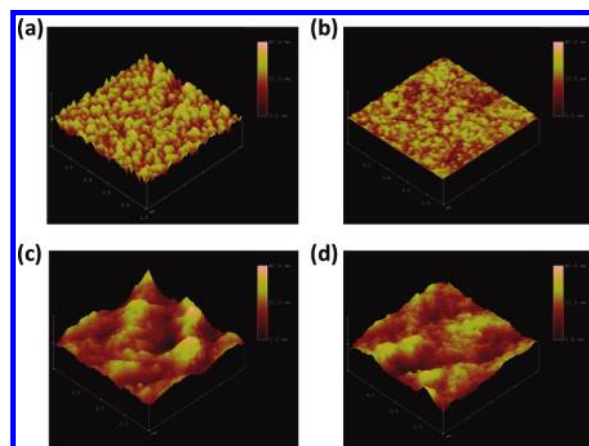


Figure 2. AFM tapping mode height images of the surface of bare ZnO (a) and a C-PCBSD thin film on top of the ZnO (b) ($1.0 \times 1.0\text{ }\mu\text{m}$) and topography images of P3HT:PCBM films on top of the C-PCBSD interlayer (c) and on top of the ZnO layer (d) after thermal annealing at $140\text{ }^\circ\text{C}$ for 10 min ($2.0 \times 2.0\text{ }\mu\text{m}$).

that the absorption intensity of the non-cross-linked layer is completely gone after rinsing with dichlorobenzene, indicating that without thermal curing, this thin layer can be totally washed out by the solvent used in the following spin coating.

The solvent resistance allows sequential active materials dissolved in dichlorobenzene to be successfully spin-coated on the C-PCBSD layer without destroying it. Unlike the case of a self-assembled monolayer C_{60} modifier, which cannot planarize the metal oxide surface, the insertion of this C-PCBSD interlayer guarantees that the upper active layer and the bottom ZnO layer can be fully separated. Finally, a solution of PEDOT:PSS was then spin-cast, followed by vacuum deposition of silver as the anode. Under identical fabrication conditions, reference device B, using an ITO/ZnO/P3HT:PCBM(1:1, w/w)/PEDOT:PSS/Ag configuration (without the C-PCBSD interlayer), was prepared for comparison. The device characteristics and $J-V$ curves of devices A and B are shown in Table 1 and Figure 3a. Under AM 1.5 G illumination at $100\text{ mW}/\text{cm}^2$, this standard device B showed a PCE of 3.5%, which agrees well with the values reported in the literature based on P3HT/PCBM blend inverted solar cells.^{5b} With an additional interlayer of C-PCBSD, the PCE of device A was substantially improved to 4.4%. This value not only represents a 26% improvement over device B but also reaches a performance comparable to that of state-of-the-art regular solar cells based on the P3HT/PCBM system. The overall improved PCE of device A is the result of its

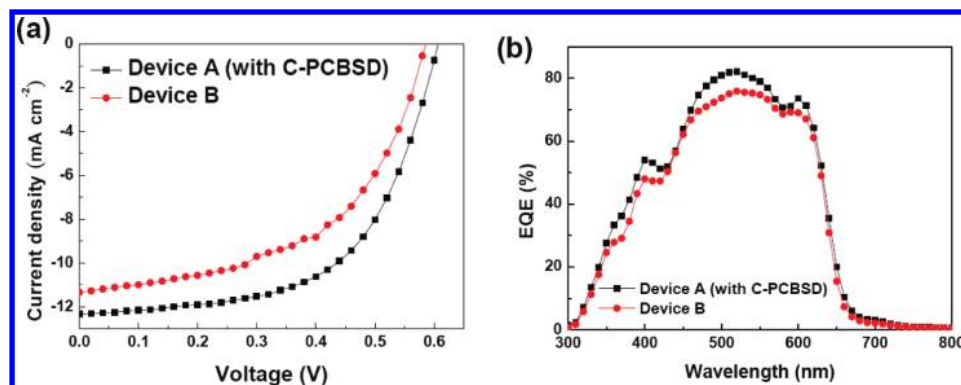
(14) (a) Zhong, H.; Yang, X.; deWith, B.; Loos, J. *Macromolecules* **2006**, *39*, 218. (b) Drees, M.; Hoppe, H.; Winder, C.; Neugebauer, H.; Sariciftci, N. S.; Schwinger, W.; Schäffler, F.; Topf, C.; Scharber, M. C.; Zhu, Z.; Gaudiana, R. *J. Mater. Chem.* **2005**, *15*, 5158.

(15) (a) O'Brien, S.; Koh, L. H. K.; Crean, G. M. *Thin Solid Films* **2008**, *516*, 1391. (b) Musat, V.; Rego, A. M.; Monteiro, R.; Fortunato, E. *Thin Solid Films* **2008**, *516*, 1512.

Table 1. Characteristics of devices A-F^a

device ^b	V_{oc} (V)	J_{sc} (mA cm ⁻²)	FF (%)	η (%) ^c	R_{sh} (Ω cm ²)	R_s (Ω cm ²)	rectification ratio
A	0.60	12.8	58	4.4(\pm 0.12)	553	5.9	
B	0.58	11.6	52	3.5(\pm 0.18)	292	6.2	
C	0.50	1.24	50	0.31(\pm 0.19)	2913	14.8	5.1×10^2
D	0.36	0.21	32	0.02(\pm 0.10)	1309	28.4	5.6×10^1
E	0.66	14.5	35	3.4(\pm 0.26)	94	10.7	
F	0.48	12.1	32	1.9(\pm 0.14)	77	10.1	

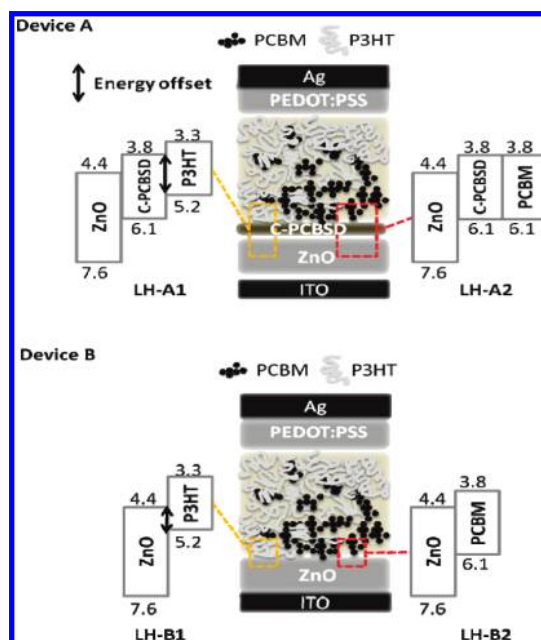
^a Definitions: open-circuit voltage, V_{oc} ; short-circuit current, J_{sc} ; fill factor, FF; PCE, η ; shunt resistance, R_{sh} ; series resistance, R_s . ^b Configurations: device A, ITO/ZnO/C-PCBSD/P3HT:PCBM(1:1, w/w)/PEDOT:PSS/Ag; device B, ITO/ZnO/P3HT:PCBM(1:1, w/w)/PEDOT:PSS/Ag; device C, ITO/ZnO/C-PCBSD/P3HT/PEDOT:PSS/Ag; device D, ITO/ZnO/P3HT/PEDOT:PSS/Ag; device E, ITO/ZnO/C-PCBSD/PCPDTBT:PC₇₁BM(1:2, w/w)/PEDOT:PSS/Ag; device F, ITO/ZnO/PCPDTBT:PC₇₁BM(1:2, w/w)/PEDOT:PSS/Ag. ^c All the performance parameters were averaged over 10 devices. The standard deviations of the PCEs are shown in parentheses.

**Figure 3.** (a) J - V curves of devices A and B under AM 1.5 G illumination at 100 mW/cm². (b) IPCE spectra of devices A and B.

simultaneously enhanced open-circuit voltage (V_{oc}), short-circuit current (J_{sc}), and fill factor (FF) relative to device B.

Because the BHJ active layer contains a p-type P3HT and an n-type PCBM component, both P3HT and PCBM domains at the interface are expected to make contact with the bottom layer to form two types of localized heterojunction at nanoscale size. Therefore, device A contains P3HT/C-PCBSD (denoted as LH-A1) and PCBM/C-PCBSD (LH-A2) localized heterojunctions at the interface, whereas device B has P3HT/ZnO (LH-B1) and PCBM/ZnO (LH-B2) at the interface (Figure 4).

To carefully analyze the characteristic differences between devices A and B, we first consider only the microscopic heterojunctions LH-A1 and LH-B1, at which the P3HT domain in the active layer is exposed to the bottom layer in the interface. First, in device A, the C-PCBSD interlayer provides an extra P3HT/C-PCBSD interface area for ultrafast exciton dissociation, which is more efficient than the P3HT/ZnO interface in device B.¹⁶ Second, the LUMO energy level of C-PCBSD (3.8 eV) is located between the LUMO of P3HT (3.3 eV) and the conduction band of ZnO (4.4 eV). Therefore, the C-PCBSD can function as an energy gradient intermediate, so that electrons can be efficiently transported to the ZnO through an energetically downhill cascade pathway.¹⁷ These advantages might be associated with the improvement in J_{sc} from 11.6 mA cm⁻² in device B to 12.8 mA cm⁻² in device A. Third, considering that the energy offset between the conduction band of ZnO and the HOMO energy of P3HT (5.2 eV) is only 0.8 eV, charge recombination at the P3HT/ZnO interface in device B is thus very likely. With n-type C-PCBSD acting as a hole-blocking

**Figure 4.** Schematic illustration of the multilayer inverted solar cell ITO/ZnO/P3HT:PCBM(1:1, w/w)/PEDOT:PSS/Ag with (device A) and without (device B) a C-PCBSD interlayer. Device A contains two localized heterojunctions, LH-A1 and LH-A2, at the active layer interface, whereas device B has LH-B1 and LH-B2 at the interface. The architectures of devices A and B, with energy diagrams of the four localized heterojunctions at the interfaces, are shown.

buffer layer in device A, back electron transfer from ZnO to either the C-PCBSD interlayer or P3HT in the active layer can be greatly suppressed, which in turn helps enhance V_{oc} and FF in device A. Although charge recombination is also possible at the P3HT/C-PCBSD interface in device A, the much larger

(16) (a) Beek, W. J. E.; Wienk, M. M.; Janssen, R. A. J. *Adv. Funct. Mater.* **2006**, *16*, 1112. (b) van Hal, P. A.; Christiaans, M. P. T.; Wienk, M. M.; Kroon, J. M.; Janssen, R. A. J. *J. Phys. Chem. B* **1999**, *103*, 4352.

(17) Niu, Y.-H.; Liu, M. S.; Ka, J. W.; Jen, A. K.-Y. *Appl. Phys. Lett.* **2006**, *88*, 093505.

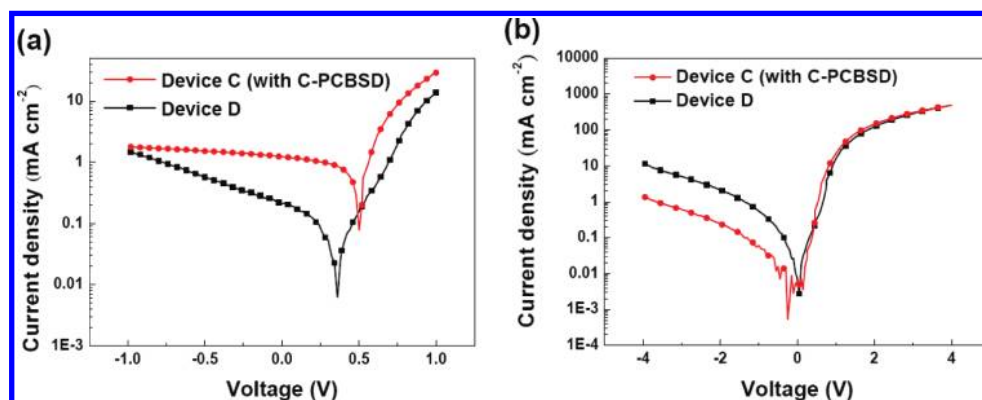


Figure 5. Semilogarithmic plots of J – V characteristics of heterojunction solar cell devices C and D (a) under AM 1.5 G illumination at 100 mW/cm^2 and (b) in the dark.

energy offset of 1.4 eV at this interface, compared to 0.8 eV at P3HT/ZnO in device B, is still beneficial for reducing its probability.

To prove the aforementioned multifunctionality of the C-PCBSD interlayer in device A, planar heterojunction device C (ITO/ZnO/C-PCBSD/P3HT/PEDOT:PSS/Ag) and device D (ITO/ZnO/P3HT/PEDOT:PSS/Ag) were fabricated and investigated. Because such a simplified bilayer heterojunction completely eliminates the influence of PCBM in the active layer, so that the exciton dissociation and charge recombination sites are located mainly at the interface of the heterojunction, the macroscopic characteristics of devices C and D can reflect the microscopic properties of LH-A1 in device A (P3HT/C-PCBSD/ZnO) and LH-B1 in device B (P3HT/ZnO), respectively.

Figure 5a shows the J – V characteristics of the planar heterojunction devices under AM 1.5 G illumination. As expected, device C showed dramatic improvement in all device characteristics relative to device D (Table 1). The significantly increased J_{sc} value verifies that the exciton dissociation efficiency of the P3HT/C-PCBSD interface in device C is much higher than that of P3HT/ZnO in device D. Again, the charge recombination kinetics depends strongly on the energy offset at the n-type/p-type bilayer heterojunction. In comparison to device D with a V_{oc} value of 0.36 V and an FF value of 32%, an enlarged energy offset in device C reduces the carrier recombination rate and appreciably improves the V_{oc} value to 0.5 V and the FF value to 50%. The J – V characteristics of devices C and D in the dark were also investigated (Figure 5b). Device C, with a C-PCBSD interlayer, showed a significant reduction in dark current under reverse bias, leading to a diode rectification ratio (current density at 3 V divided by current density at -3 V) higher by an order of magnitude than for device D (5.1×10^2 vs 5.6×10^1). This result may suggest that the C-PCBSD interlayer in device C can indeed passivate the local shunts at the ZnO interface and therefore block the injection of holes in the leakage pathways of the ZnO. This is also supported by the much increased shunt (parallel) resistance (R_{sh}) of devices A ($553 \Omega \text{ cm}^2$) and C ($2913 \Omega \text{ cm}^2$) compared to their reference devices B ($292 \Omega \text{ cm}^2$) and D ($1309 \Omega \text{ cm}^2$), respectively (Table 1). Consequently, the reduced leakage current leads to improved V_{oc} and FF values in device C.

After examining LH-A1 in device A and LH-B1 in device B, we further consider the microscopic properties of another localized heterojunction, PCBM/C-PCBSD (LH-A2) in device A and PCBM/ZnO (LH-B2) in device B (Figure 4). The electrochemical properties of the PCBSD were studied by cyclic voltammetry (Figure S3 and Table S1). It is not surprising to

observe that the chemically modified PCBSD has a LUMO energy level very similar to that of its parent PCBM (3.8 eV), thus forming ohmic contact with PCBM in the active layer of device A. In comparison to ZnO, which acts as an inorganic electron-selective layer in device B, the C-PCBSD interlayer in device A serves as an organic electron-selective layer. The obvious advantage of device A over device B is that the ohmic contact and organic–organic interface can enhance electrical coupling and lower the contact resistance, facilitating electron transport through the interface. As a result, electrons in the PCBM domain can be effectively extracted by the C-PCBSD interlayer from the active layer, where recombination is apt to take place due to directionless charge transport. Even though the bulk resistance as a result of the additional C-PCBSD layer may increase the series resistance (R_s), the overall series resistance of device A ($5.9 \Omega \text{ cm}^2$) is still smaller than that of device B ($6.2 \Omega \text{ cm}^2$), implying that the C-PCBSD interlayer is indeed capable of reducing the contact resistance in device A.

To investigate the effect of the C-PCBSD interlayer on the morphology of the sequential active layer, AFM images under the tapping mode were used to trace differences in the surface topography of the P3HT:PCBM overlayer on ZnO and on C-PCBSD. After thermal annealing at 140°C for 10 min, the P3HT:PCBM layer on C-PCBSD showed a higher surface roughness of 4.61 nm (Figure 2c) compared to that on the ZnO surface with a roughness of 3.06 nm (Figure 2d). Due to the excellent compatibility and strong affinity between PCBM and C-PCBSD as well as the lower surface energy of P3HT, the active layer deposited on C-PCBSD tends to adopt a vertical phase separation in which the bottom side is PCBM-rich and the upper side is P3HT-rich. Therefore, the higher ordering of the P3HT domain close to the top surface leads to greater surface roughness. In addition, a comparison of the incident photon to current efficiency (IPCE) spectra (Figure 3b) shows that device A exhibits a more pronounced vibronic shoulder around 610 nm, indicating a higher degree of P3HT crystallinity, than device B. This type of distribution of n-type and p-type materials in the active layer is ideal for inducing directional charge carrier transportation in inverted solar cells.¹⁸

(18) (a) Campoy-Quiles, M.; Ferenczi, T.; Agostinelli, T.; Etchegoin, P. G.; Kim, Y.; Anthopoulos, T. D.; Stavrinou, P. N.; Bradley, D. D. C. *Nat. Mater.* **2008**, *7*, 158. (b) Xu, Z.; Chen, L.-M.; Yang, G.; Huang, C.-H.; Hou, J.; Wu, Y.; Li, G.; Hsu, C.-S.; Yang, Y. *Adv. Funct. Mater.* **2009**, *19*, 1227. (c) Kumar, A.; Li, G.; Hong, Z.; Yang, Y. *Nanotechnology* **2009**, *20*, 165202.

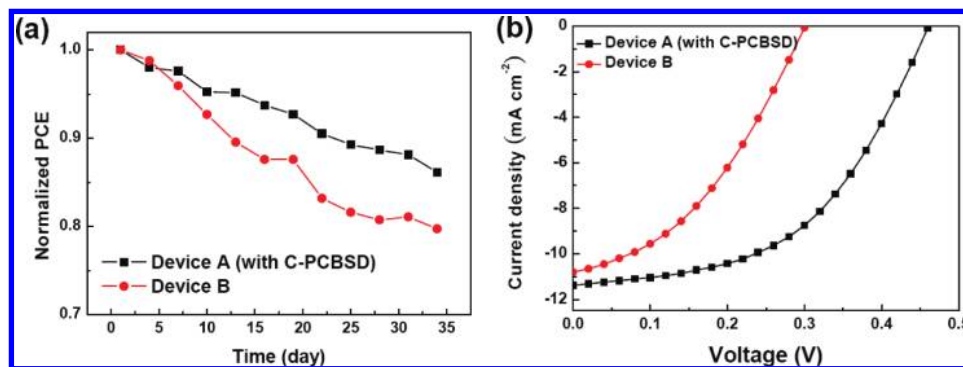


Figure 6. (a) Normalized PCEs as a function of time for devices A and B stored for 35 days in air under ambient conditions. (b) J - V curves of devices A and B under AM 1.5 G illumination at 100 mW/cm^2 after -5 V reverse bias stressing at a frequency of 2 Hz for 5 h .

The PCEs of the unencapsulated inverted solar cell devices A and B were periodically measured for 35 days to monitor their long-term stability (Figure 6a). Device B retains 80% of the magnitude of its original PCE value after being exposed to ambient conditions for 35 days. In sharp contrast, the device performance of a regular solar cell (ITO/PEDOT:PSS/PCBM: P3HT/Ca/Al) without encapsulation decays very rapidly in just 2 days. This explicitly demonstrates the superior air stability of inverted solar cells. Most encouragingly, device A exhibited even better long-term stability than device B. The device degradation rate was quantified by plotting normalized PCEs as a function of time; the slopes were $4.1 \times 10^{-3} \text{ day}^{-1}$ for device A and $6.6 \times 10^{-3} \text{ day}^{-1}$ for device B (using the least-squares method). This result indicates that the C-PCBSD interlayer plays a key role in increasing the lifetime of device A by 1.5 times relative to that of device B.

Note that for most practical applications, a number of single cells must be connected in series to form a module producing sufficient voltage. Under illumination, if a single cell in the module is shaded and cannot absorb light, it is forced to be under reverse bias driven by the other illuminated cells to generate electrical power. Therefore, it is also crucial to evaluate the stability of a single cell under the influence of reverse bias. For this reason, we applied a voltage pulse of -5 V to devices A and B at a frequency of 2 Hz for 5 h under ambient conditions and then remeasured the J - V characteristics under AM 1.5 G at 100 mW/cm^2 (Figure 6b). The PCE of device B dropped significantly to 1.2%, corresponding to a 66% loss of its original value prior to reverse bias stressing, whereas device A exhibited better stability against reverse bias, showing a 40% decay to obtain a much higher PCE of 2.6%. Device degradation is known to be related to leakage current caused by the formation of hot spots in bulk or at the interface.¹⁹ The coverage of a three-dimensional C-PCBSD network on ZnO might passivate the hot spots generated in the ZnO to suppress the leakage current, thus improving the operational lifetime. Additionally, without this interlayer as a dense and robust spacer, gradual mutual penetration between the ZnO and the active layer in device B may alter their chemical or physical properties as the operational time increases.

While recent research on inverted solar cells has concentrated mainly on device engineering on the basis of the typical P3HT/PCBM system, the use of other low band gap p-type polymers has not been well explored due to their relatively low device performance. After successfully demonstrating that a C-PCBSD

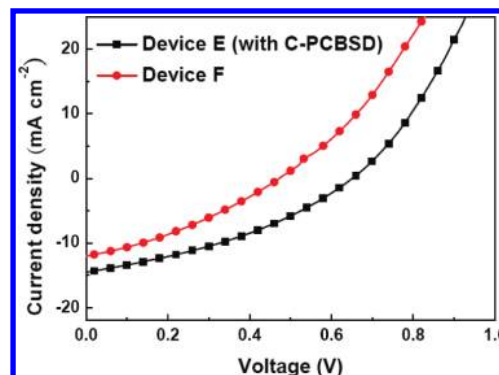


Figure 7. J - V curves of devices E and F under AM 1.5 G illumination at 100 mW/cm^2 .

interlayer can effectively improve the performance of a P3HT/PCBM-based inverted solar cell, we envision that this strategy can be a general approach for extension and application to other blending systems using a low-band-gap polymer with better light-harvesting ability. A well-studied p-type polymer, poly[2,6-(4,4-bis(2-ethylhexyl)-4*H*-cyclopenta[2,1-*b*;3,4-*b'*]dithiophene)-*alt*-4,7-(2,1,3-benzothiadiazole)] (PCPDTBT), with a band gap of 1.4 eV , was chosen to test this idea.²⁰ Device E (ITO/ZnO/C-PCBSD/PCPDTBT:PC₇₁BM (1:2, w/w)/PEDOT:PSS/Ag) and its corresponding reference device F without the C-PCBSD interlayer (ITO/ZnO/PCPDTBT:PC₇₁BM (1:2, w/w)/PEDOT:PSS/Ag) were therefore fabricated. Encouragingly, device E exhibited a V_{oc} value of 0.66 V , a J_{sc} value of 14.52 mA cm^{-2} , and an FF value of 35.4%, leading to a PCE value of 3.4%, which is a considerable improvement of 78% compared to device F (PCE = 1.9%) without this C-PCBSD interlayer (Table 1 and Figure 7). The PCE of 3.4% again achieves a level comparable to that of a regular solar cell based on the PCPDTBT:PC₇₁BM system.¹⁸ To the best of our knowledge, this is the first example of an inverted solar cell using a low-band-gap polymer other than P3HT that can obtain a PCE greater than 3%.

Conclusion

In conclusion, a novel PCBM-based n-type material, PCBSD, functionalized with a dendron containing two styryl groups as the thermal cross-linkers, has been rationally

(19) Steim, R.; Choulis, S. A.; Schilinsky, P.; Lemmer, U.; Brabec, C. J. *Appl. Phys. Lett.* **2009**, *94*, 043304.

(20) (a) Zhu, Z.; Waller, D.; Gaudiana, R.; Morana, M.; Mühlbacher, D.; Scharber, M.; Brabec, C. J. *Macromolecules* **2007**, *40*, 1981. (b) Chen, C.-H.; Hsieh, C.-H.; Dubosc, M.; Cheng, Y.-J.; Hsu, C.-S. *Macromolecules* **2010**, *43*, 697.

designed and easily synthesized. In situ cross-linking of PCBSD was carried out by heating at a low temperature of 160 °C for 30 min to achieve a robust and solvent-resistant network, enabling the fabrication of a multilayer inverted device by solution processing. This C-PCBSD interlayer has multiple positive effects on both n-type semiconductor/C-PCBSD and p-type semiconductor/C-PCBSD localized heterojunctions at the interface of the active layer as well as the interface of ZnO. An inverted solar cell device based on the ITO/ZnO/C-PCBSD/P3HT:PCBM/PEDOT:PSS/Ag configuration not only demonstrates enhanced device characteristics, with an impressive PCE of 4.4%, but also possesses exceptional device lifetime without encapsulation, overcoming the stability–performance trade-off. Moreover, this promising approach can be applied to another inverted solar cell system using PCPDTBT/PC₇₁BM as the active layer to

achieve an improved PCE of 3.4%. We envision that incorporation of the cross-linked C₆₀ interlayer could become a standard procedure in the fabrication of highly efficient and stable multilayer inverted solar cells.

Acknowledgment. This work is supported by the National Science Council and “Aim for the Top University Plan” of the National Chiao Tung University and Ministry of Education, Taiwan.

Supporting Information Available: Text, figures, and a table giving synthetic procedures, device fabrication details, DSC, contact angle, and cyclic voltammetry measurements, and ¹H and ¹³C NMR spectra. This material is available free of charge via the Internet at <http://pubs.acs.org>.

JA100236B